Stability of Elastomeric Isolation Bearings: Experimental Study

Ian Buckle[1]; Satish Nagarajaiah[2]; and Keith Ferrell[3]

Abstract: Elastomeric isolation bearings are required to be stable at high shear strains, which occur during strong earthquakes. Hence, rigorous determination of the critical axial load during design is important. Currently, the critical load is determined using the small displacement Haringx theory and modified to account for large shear strains by an approximate correction factor. The objective of this study is to experimentally determine the effect of horizontal displacement or shear strain on critical load and to study the validity of the approximate correction factor. Experiments were conducted on a series of elastomeric bearings with low shape factors. Test procedure and test results are presented in detail. It is shown that the critical load decreases with increasing horizontal displacement or shear strain. It is also shown that substantial critical load capacity exists at a horizontal displacement equal to the width of the bearing and is not zero, as predicted by the correction factor. It is further shown that the approximate formula is not conservative at smaller displacements and overly conservative at larger displacements. The critical loads obtained from experiments are compared with results from finite element analyses and nonlinear analytical solutions; the comparisons indicate that the effect of large horizontal displacements on the critical load can be reliably predicted.

DOI: 10.1061/(ASCE)0733-9445(2002)128:1(3)

CE Database keywords: Seismic isolation; Stability; Experimentation; Shear strain; Axial loads; Critical loads.

Introduction

An elastomeric isolation bearing consists of a number of rubber layers and steel shims, bonded in alternating layers, to produce a vertically stiff but horizontally flexible isolator. This flexibility lengthens the fundamental period of the isolated building and reduces the seismic forces in the superstructure. But this reduction may be accompanied by large horizontal displacements in the isolators, which, together with their lateral flexibility, may lead to significant reduction in their critical axial load (Buckle and Kelly 1986; Koh and Kelly 1986; Buckle and Liu 1994; Nagarajaiah and Ferrell 1999).

The design approach used currently to compute the critical load, P_{cro}, at small displacements is to use Haringx's theory (1948, 1949a,b):

$$P_{cro}=\frac{(GA_s)_{eff}}{2}\left[\sqrt{1+4\frac{P_E}{(GA_s)_{eff}}}-1\right] \quad (1)$$

where $P_E=\pi^2(EI)_{eff}/l^2$; $(GA_s)_{eff}$=effective shear rigidity and $(EI)_{eff}$ is the effective flexural rigidity; E is the bending modulus; and G is the shear modulus of rubber. The following relations (Buckle and Kelly 1986; Koh and Kelly 1986) can be used to establish the effective shear rigidity and effective flexural rigidity.

$$(GA_s)_{eff}=GA(l/l_r) \quad (2)$$

$$(EI)_{eff}=E_rI(l/l_r) \quad (3)$$

where l=combined height of the rubber layers and steel plates, excluding the top and bottom plates; l_r=total thickness of all rubber layers=Σt (t=rubber layer thickness); A=bonded rubber area; and I=moment of inertia of the bearing about the axis of bending,

$$E_r=E_0(1+0.742\,S^2) \quad (4)$$

where E_0=elastic modulus of rubber, which is approximately equal to four times the shear modulus, G, and S, the shape factor, is defined as

$$S=\frac{\text{loaded area of rubber layer}}{\text{force-free area of rubber layer}} \quad (5)$$

Currently, the effect of large horizontal displacements is accounted for approximately by reducing the value of the critical load, P_{cro}, using a correction factor equal to the ratio of effective column area and actual column area at large horizontal displacement (Buckle and Liu 1993). For a rectangular bearing, this factor gives the following value for P_{cr}:

$$P_{cr}=P_{cro}[1-\Delta/B] \quad (6)$$

where P_{cr}=critical load at horizontal displacement, Δ; P_{cro} =critical load given by Haringx's theory; and B=bearing width.

The horizontal stiffness is dependent on the axial load, and can be approximated by (Buckle and Kelly 1986):

$$K_h=K_h^*\left[1-\left(\frac{P}{P_{cr}}\right)^2\right] \quad (7)$$

[1]Professor, Dept. of Civil Engineering, Univ. of Nevada, Reno, NV 89557.

[2]Associate Professor, Dept. of Civil Engineering, Rice Univ. Houston, TX 77005. E-mail: nagaraja@rice.edu

[3]Engineer, Dept. of Transportation, Jefferson City, MO 65102

Note. Associate Editor: Brad Cross. Discussion open until June 1, 2002. Separate discussions must be submitted for individual papers. To extend the closing date by one month, a written request must be filed with the ASCE Managing Editor. The manuscript for this paper was submitted for review and possible publication on December 21, 2000; approved on June 15, 2001. This paper is part of the ***Journal of Structural Engineering***, Vol. 128, No. 1, January 1, 2002. ©ASCE, ISSN 0733-9445/2002/1-3–11/$8.00+$.50 per page.

where P = axial load; K_h^* = horizontal stiffness at zero axial load, and K_h = modified horizontal stiffness.

The experimental study presented in this paper involves tests on elastomeric bearings in order to investigate the variation of critical load with horizontal displacement or shear strain. Test procedure and test results are presented in detail. The validity of the approximate result in Eq. (6) is evaluated. Comparisons of experimental results with ADINA finite element analysis results of Liu et al. (personal communication, 2001) are presented. In a companion paper, Nagarajaiah and Ferrell (1999) developed a nonlinear analytical model and verified it using the experimental results presented in this study. The comparisons with the results of the nonlinear analytical model are also presented.

Bearings Tested

The multilayer elastomeric bearings tested consist of natural rubber layers and steel shims bonded in alternating layers as shown in Fig. 1(a). A total of 12 bearings were tested. Nine of the square bearings were five in. by five in. (127 mm × 127 mm) in plan. Three of the square bearings were ten in. by ten in. (254 mm × 254 mm) in plan. Bearing properties are shown in Table 1 and Fig. 1(a); the 10 in. bearing properties are shown in parentheses. All bearings had bolted connections at the top and bottom to prevent overturning. The rubber layer thickness was varied in order to study bearings with different shape factors. This thickness is typically less than 0.5 in. (12.7 mm); However, four of the bearing series tested (100, 200, 400, and 500) had layer thicknesses greater than or equal to 0.5 in. (12.7 mm), to study the effect of low shape factor or increased slenderness. The 300 series and 600 series of bearings had 0.25 in. (6.35 mm) rubber layer thickness. The rubber shear modulus, G, was estimated to be 0.2 ksi (1.38 MPa) at 0% shear strain and 0.136 ksi (0.938 MPa) at 100% shear strain (Nagarajaiah and Ferrell 1999). The rubber cover was 0.125 in. (3.18 mm) thick for all bearings. The steel shim thickness was varied in order to maintain the same overall height. All bearings tested had 1 in. (25.4 mm) thick end plates.

Test Setup

The elastomeric bearings were tested using the uniaxial single bearing test facility at the Earthquake Engineering Research Center at the Univ. of California at Berkeley [see Figs. 1(a and b)]. The test setup permitted simultaneous application of vertical and horizontal loads. The two vertical actuators on either side of the bearing [See Fig. 1(b)] generated the vertical load. During testing, the load in each actuator was adjusted to maintain the required vertical load taking into account the overturning moment in the bearings and the increasing inclination of actuators (from the vertical) as the horizontal displacement increases. A similar correction was also necessary to the horizontal actuator with increasing shear displacements.

The test was run with the horizontal actuator under displacement control and the vertical actuator under force control, i.e., the horizontal displacement was held at a specified value while the vertical load was increased until critical load conditions occurred. For the purpose of this experiment, a bearing was considered to be in critical state when the horizontal force became zero or negative. Horizontal forces and vertical displacements were therefore monitored throughout the test. This protocol assured the safety of the test system as critical conditions were approached.

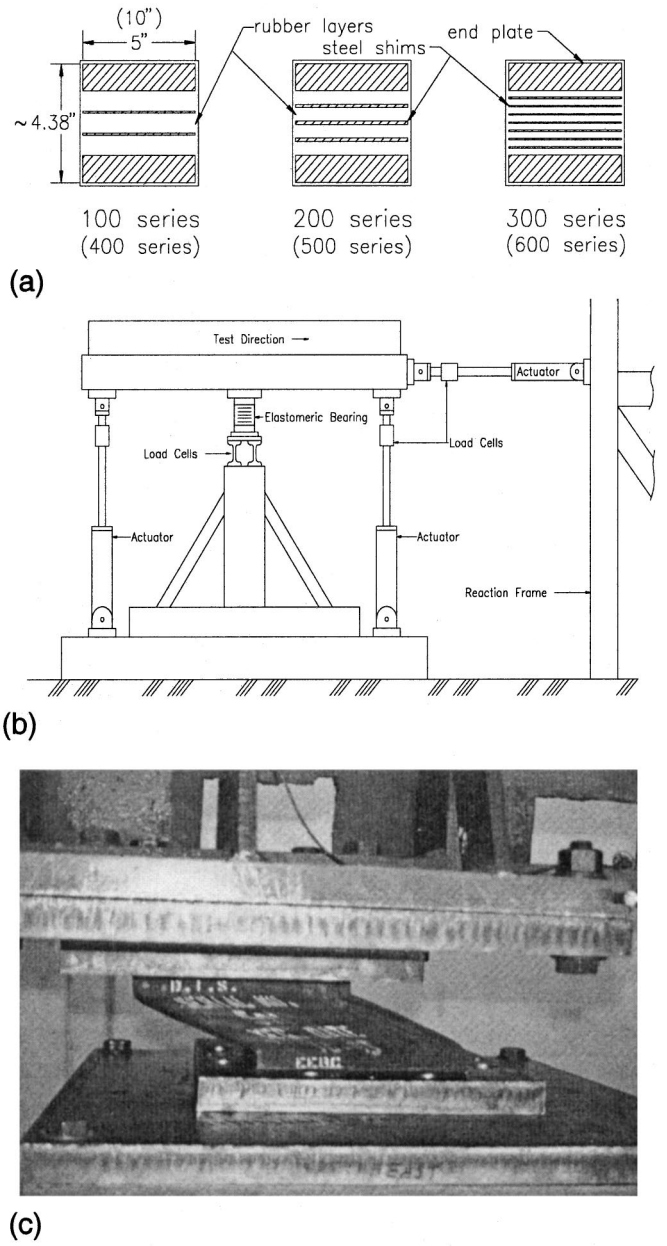

Fig. 1. (a) Details of elastomeric bearings tested; (b) uniaxial single bearing test rig; and (c) 10 in. bearing displaced to 0.6B in test rig

Test Procedure

Fifteen channels were used to record and monitor data collected at a sampling frequency of 50 Hz. The test sequence involved five cycles of scrag test, five cycles of shear test 1, monotonic stability test, and five cycles of shear test 2. The testing procedure is summarized below. For a predetermined shear displacement, u, (for example, 0.2B, B = width of the square bearing) the following sequence of tests were performed:

1. Scrag test (Cyclic test)
   - Constant axial load $P = P_1$ applied,
   - Five cycles of shear displacement, $\pm u$, applied.
2. Shear test 1 (Cyclic test)
   - A constant axial load $P = P_1$ applied,
   - Five cycles to shear displacement, $\pm u$, applied.
3. Stability/critical load test (quasistatic test) as shown in Figs. 2(a and b)

Table 1. 5 and 10 in. Elastomeric Bearing Details[a]

Bearings tested	Nominal size $B\times B'\times H$[b] (in.×in.×in.)	Number of rubber layers	Thickness of rubber layers (In.)	Thickness of steel shim (In.)	Shape factor
101, 102, 103	5×5×4.375	3	0.75	0.0625	1.67
201, 202, 203	5×5×4.375	4	0.50	0.1250	2.50
301, 302, 303	5×5×4.385	8	0.25	0.0550	5.00
401	10×10×4.375	3	0.75	0.0625	3.33
501	10×10×4.375	4	0.50	0.1250	5.00
601	10×10×4.385	8	0.25	0.0550	10.00

[a]1 in.=2.54 mm.

[b]B=width of the square bearing, B'=breadth; H=height of the bearing.

- Axial load $P=P_1$ applied. $P_1=5$, 10, 20, 80, 80, 80 kip for 100, 200, 300, 400, 500, and 600 series, respectively [1 kip=4.448 kN],
- Predetermined initial displacement, u, applied and held,
- The axial load, P, increased monotonically until the horizontal force, F, became negative,
- The horizontal displacement brought to zero by unloading.

4. Shear test 2 (Cyclic test)
   - Constant axial load $P=P_1$ applied,
   - Five cycles to shear displacement, $\pm u$, applied.

Steps 1–4 were repeated for the same bearing with a different initial displacement, u, of $0.2B$, $0.4B$, $0.6B$, $0.8B$, $1.0B$, and $1.2B$. The scrag and shear tests were essentially the same, except, that the purpose of the scrag test was to precondition the bearing until steady state bearing properties were achieved. The shear tests were repeated to observe changes in bearing properties, before and after each stability test. While the scrag and shear tests were conducted under constant axial load and cyclic shear displacement, the quasistatic stability tests were conducted with constant displacement and monotonically varying axial load.

Test Results

The results of the critical load tests are highlighted in this paper. The time histories of horizontal displacement, u, axial load, P, and shear force, F, are shown in Fig. 2(a). From Fig. 2(a) it is evident that as the axial force, P, is increased, the shear force, F, decreases and becomes negative, while the horizontal displacement remains at $+u$.

Fig. 2(b) shows the variation of shear force, F, with increasing axial load, P, for each test performed at a predetermined displacement $u=0.2B$, $0.4B$, $0.6B$, $0.8B$, and $1.0B$, for bearing 302. It is shown that, for a given displacement, u, as the axial load, P, is increased the shear force decreases until it becomes negative.

Determination of Critical Load from Test Results

In the preliminary evaluation of test results the critical loads were estimated using the data in Fig. 2(b) and following procedure: the value of the axial load at which the horizontal load is zero was defined as the critical load for that shear displacement. This procedure gives ''constrained'' critical loads, in that the bearing is held against further horizontal displacements as the critical load is approached (Buckle and Liu 1994). These boundary conditions are not typical of those used in practice where the horizontal displacement is unconstrained and free to increase as necessary. Upon further analysis of the test data, using a new and accurate procedure developed by Nagarajaiah and Ferrell (1999) based on equilibrium paths, the unconstrained critical loads were determined [Nagarajaiah and Ferrell 1999; Liu et al. (personal communication (2001))] and it is these results which are presented and discussed in this paper.

The axial load—horizontal displacement, $P-u$, variation is shown in Fig. 2(c) as a function of shear force for bearing 302. The equilibrium path, a smooth curve passing through discrete points, shown in Fig. 2(c), at each shear force level, passes through a limit point, which is the critical load. In Fig. 2(c) the equilibrium paths are unstable past the limit point (Nagarajaiah and Ferrell 1999); hence, the critical load must decrease with increasing horizontal displacement. The critical load, P_{cr}, obtained from Fig. 2(c) is shown in Fig. 3(a) as a function of horizontal displacement. The shear force—horizontal displacement curves in Fig. 3(b) can be used to verify the critical load, since, at P_{cr} the horizontal tangential stiffness goes to zero.

The shear force—horizontal displacement, $F-u$, curves are shown in Fig. 3(b) as a function of axial load for bearing 302. Two important features to be noted in Fig. 3(b) are as follows: the $F-u$ curves pass through a maximum as the horizontal displacement increases, under constant axial load; the shear force and horizontal displacement at which the maximum occurs decrease with increasing axial load. In Fig. 3(b), the horizontal tangential stiffness, K_h, decreases with increasing axial load and horizontal displacement.

Evaluation of Test Results

In Fig. 3(a), it is evident that significant reduction in P_{cr} occurs at horizontal displacements equal to the width of the bearing, $B=5$ in. The error bars in Fig. 3(a) represent the variability of the recovered test results; since, the tests were performed only at 1, 2, 3, 4, and 5 in. horizontal displacements and the points in between these displacements were recovered by curve fitting techniques.

The moment—horizontal displacement, $M-u$, curves are shown in Fig. 4(a) as a function of axial load for bearing 302. The moment shown is an approximate moment, which was recovered from loadcell measurements. Since rotation measurements were not recorded, moment–rotation curves could not be generated. In Fig. 4(a) the $M-u$ curve increases with increasing axial load—a trend typically observed in moment–rotation curves of elastomeric bearings—and hence, moment resisting capability increases with increasing axial load. The moment is a nonlinear function of displacement.

The height reduction due to horizontal displacement of the bearing 302 is shown in Fig. 4(b), as a function of axial load. It is

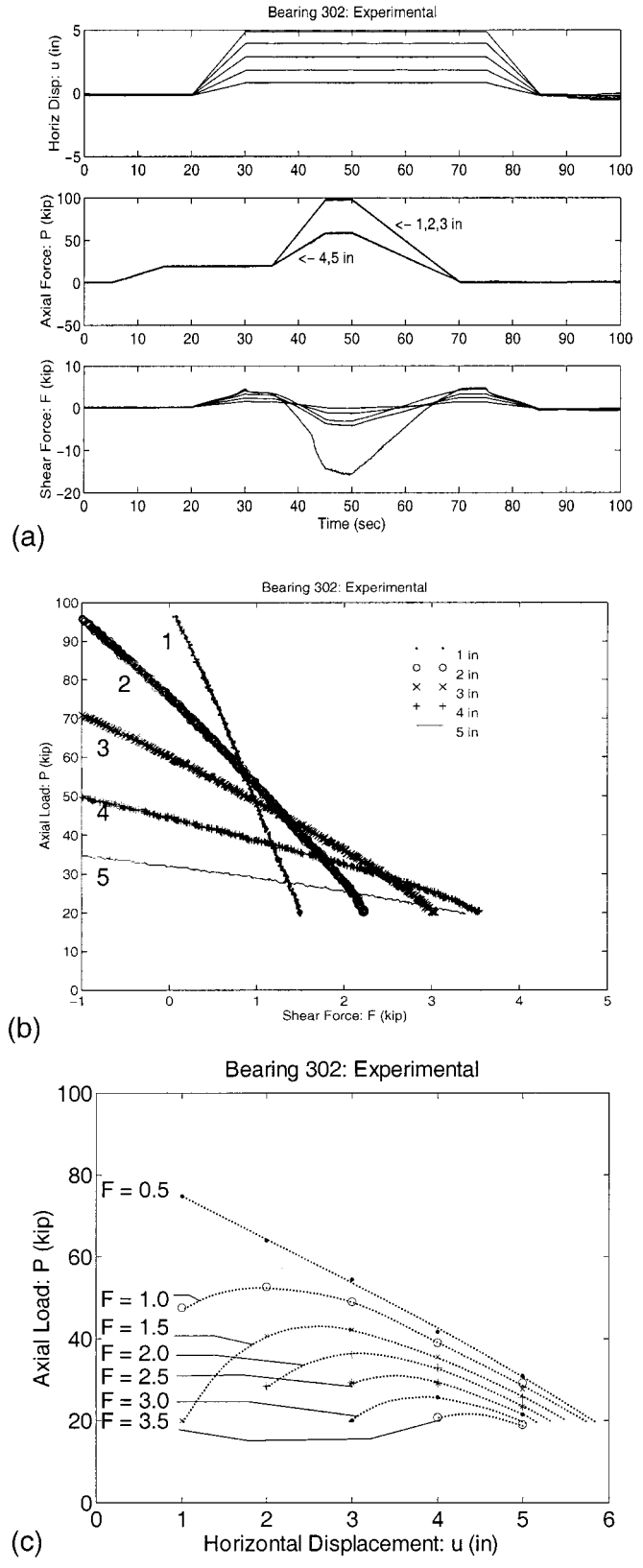

Fig. 2. Stability test: (a) Force, P, F, and displacement, u, time histories; (b) Axial load–shear force variation as function of displacement, u; and (c) Axial load–horizontal displacement variation as a function of shear force, F

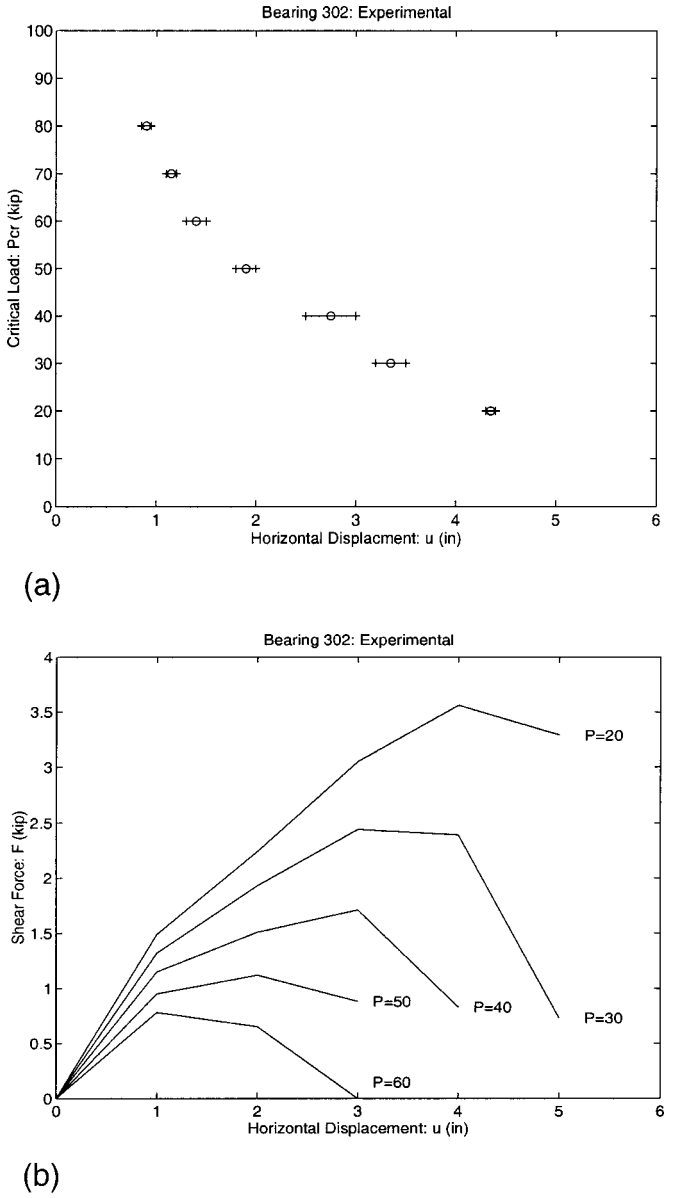

Fig. 3. Stability test: (a) Critical load as function of horizontal displacement and (b) shear force–displacement curves as function of axial load

evident from Fig. 4(b) that the height reduction increases as the horizontal displacement and axial load increase.

The variation of critical load, P_{cr}, with respect to horizontal displacement for the bearings 103 and 201 is shown in Figs. 5(a and b). Again, it can be observed from Figs. 5(a and b) that critical load decreases with increasing horizontal displacement. However, in these two sets of bearings the decrease in P_{cr} is not as significant as in bearing 302. The shear force—horizontal displacement, $F-u$, curves are shown as a function of axial load in Figs. 6(a and b). The severe nonlinearities are clearly evident in Figs. 6(a and b), similar to bearing 302.

The height reduction due to horizontal displacement of the bearings 103 and 201 is shown in Figs. 7(a and b), as a function of axial load. Again, it is evident that the height reduction increases with increasing horizontal displacement and axial load.

The shear force—horizontal displacement, $F-u$, curves are shown as a function of axial load in Fig. 8 for 10 in. bearings 401,

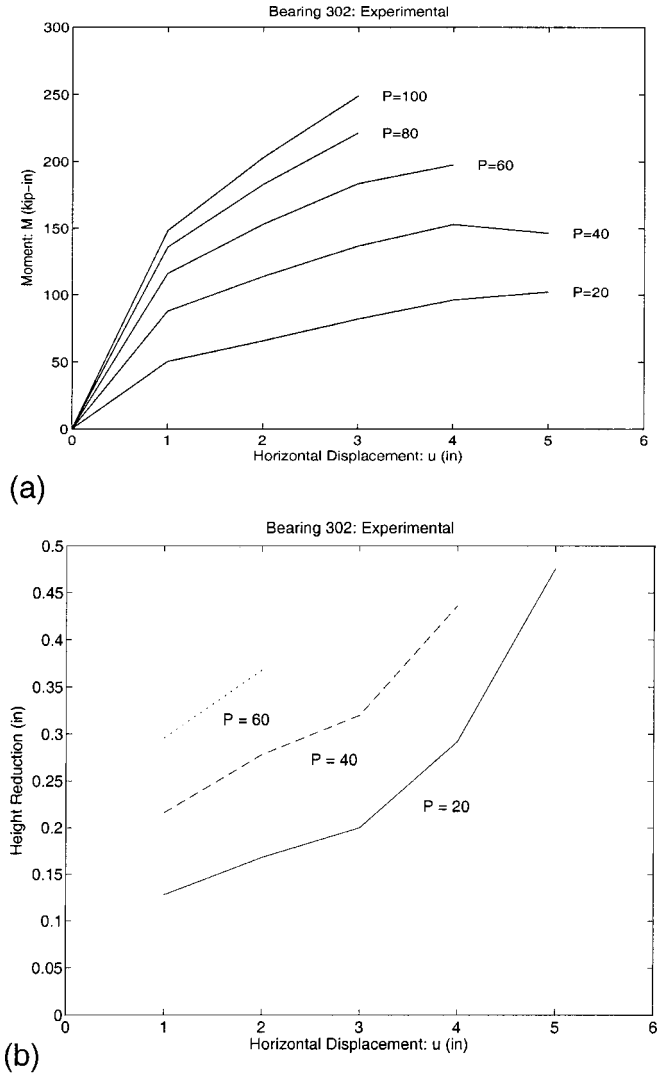

Fig. 4. Stability test: (a) Moment–displacement curves as function of axial load and (b) height reduction due to horizontal displacement as function of axial load levels for bearing 302

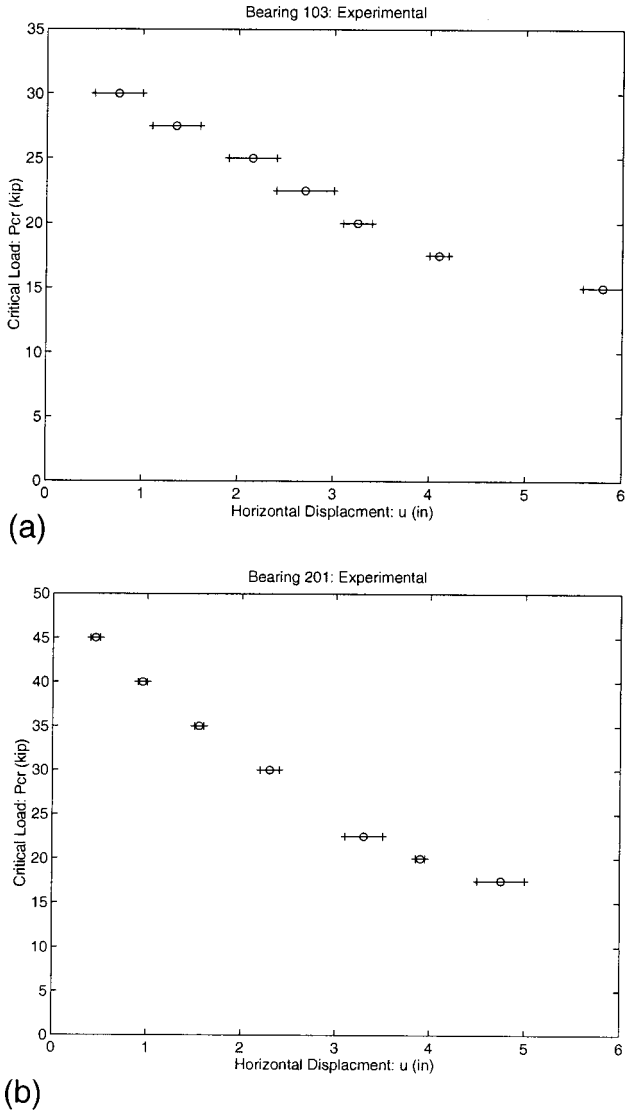

Fig. 5. Stability test: Critical load as function of horizontal displacement (a) bearing 103 and (b) bearing 201

501, and 601. The critical load variation or $P_{cr}-u$ curves could not be obtained from test results for 401, 501, and 601 series bearings because the bearings were not loaded to such high levels of axial load due to test setup limitations. From Fig. 8, a similar trend as in 5 in. bearings is observed.

Finite Element Analysis

Liu et al. (2002) have studied the stability of the elastomeric bearings tested in this study, using the ADINA (1999) finite element program. The Mooney–Rivlin material model suited for rubber undergoing large strains was adopted. In the Mooney–Rivlin model (ADINA 1999), it is assumed that the bulk modulus is several thousand times as large as the shear modulus of rubber, which is almost incompressible; this assumption is incorporated by removing the restriction that the invariant ${}_o^tI_3=1$ and including the hydrostatic term in the strain energy function to obtain

$${}_o^tW=C_1({}_o^tI_1-3)+C_2({}_o^tI_2-3)+W_H({}_o^tI_3), \qquad (8)$$

where ${}_o^tW=$ strain energy density per unit original volume; W_H = hydrostatic work term; ${}_o^tI_i=$ invariants given in terms of the components of the Cauchy–Green deformation tensor; and C_1 and $C_2=$ material constants. Modified form (ADINA 1999) of Eq. (8) used for displacement/pressure formulation is

$${}_o^t\overline{W}=C_1({}_o^tJ_1-3)+C_2({}_o^tJ_2-3)+1/2k({}_o^tJ_3-1)^2 \qquad (9)$$

where ${}_o^tJ_i=$ reduced invariants.

An incremental nonlinear analysis with an updated Lagrangian formulation was used, wherein, all kinematic nonlinearities, large displacements/rotations and large strains were accounted for. Newton–Raphson iterations were used in which both nodal point displacements and pressure variables were updated incrementally during each iteration. In order to minimize the computational effort, a plane strain restriction was imposed and the bearings were modeled as strip bearings (of unit breadth). The boundary conditions imposed were appropriate for plane strain condition. Also, fixity at the bottom plate and the top plate, free to translate horizontally and vertically but restrained against rotation, were modeled. The material properties were similar to the tested bearings: shear modulus $G=0.136$ ksi (0.938 MPa), bulk modulus K

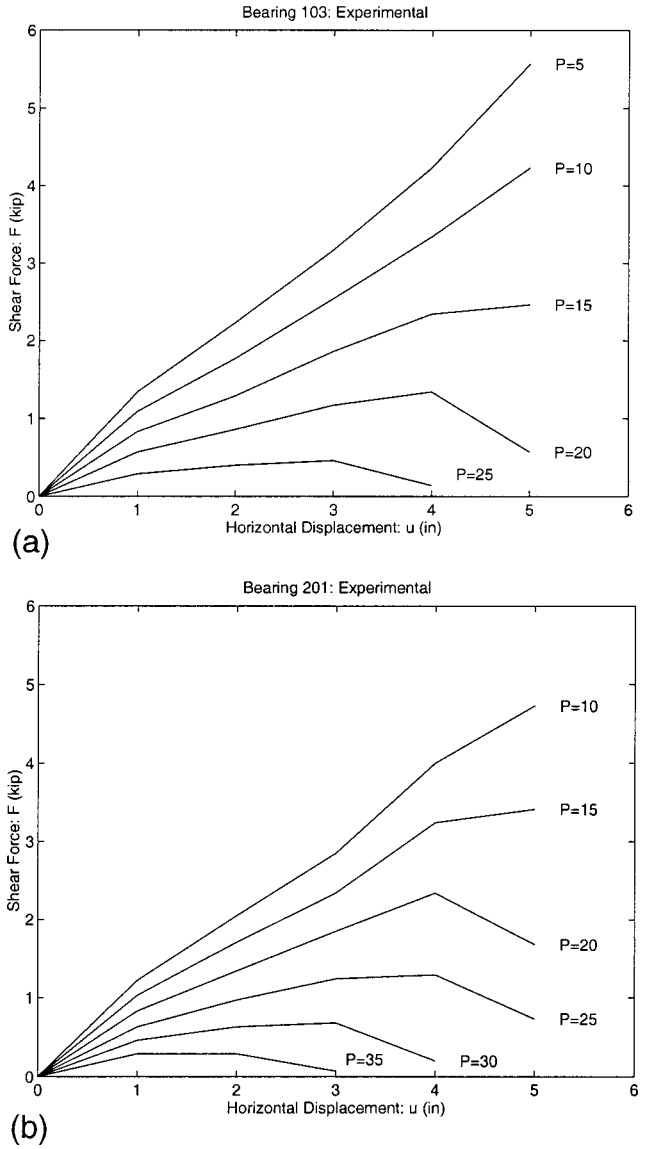

Fig. 6. Stability test: Shear force–displacement curves as function of axial load (a) bearing 103 and (b) bearing 201

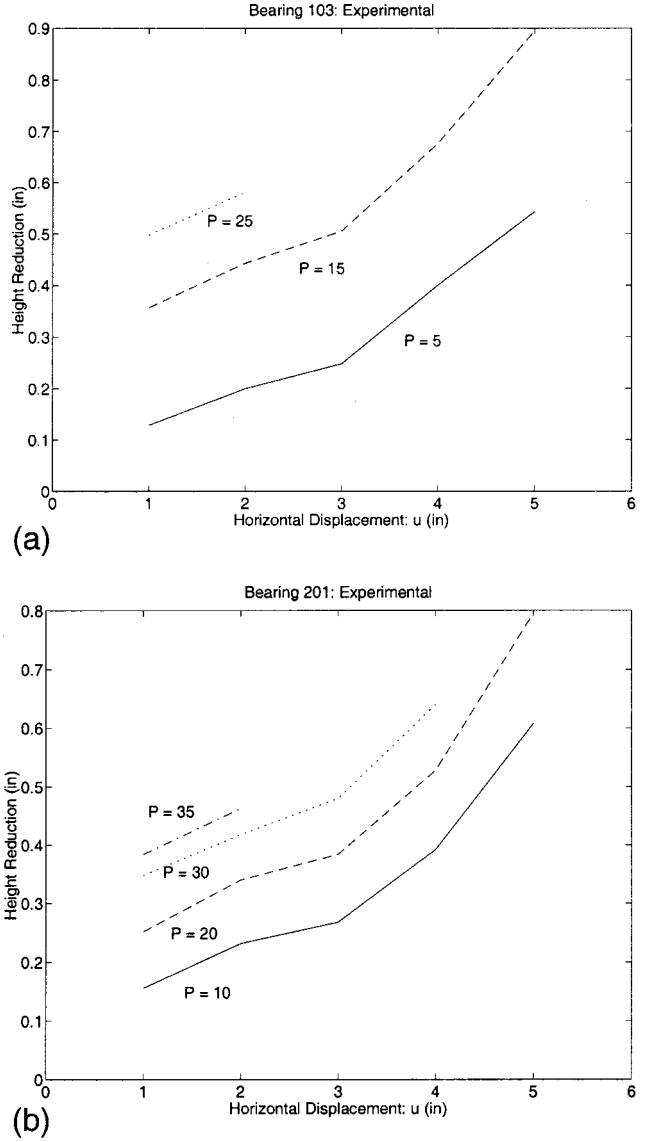

Fig. 7. Stability test: Height reduction due to horizontal displacement as function of axial load levels (a) bearing 103 and (b) bearing 201

=408, 420 ksi (2816 GPa), Poisson's ratio $\gamma = 0.499667$, and steel shim properties were Young's modulus $E_s = 30{,}000$ ksi (206.85 GPa), yield stress $\sigma_y = 44$ ksi (303.38 MPa), strain hardening modulus $E_t = 1{,}500$ ksi (10.35 GPa), and Poisson's ratio $\gamma = 0.2$. The parameters $C_1 = 0.0424$ ksi (0.292 MPa) and $C_2 = 0.0256$ ksi (0.177 MPa) were used for the Mooney–Rivlin model.

The stability of the bearings was determined by the following procedure involving equilibrium paths (Nagarajaiah and Ferrell 1999). The bearings were first deformed in shear to a predetermined shear displacement by means of a constant shear force, as shown in Fig. 9. Then, additional shear displacements were monitored as the axial load, in the form of vertical pressure at the top surface of the bearing, shown in Fig. 9, was monotonically increased up to the limit point of the equilibrium path. The equilibrium path past the limit point could not be traced as the incremental solution failed. The critical load is the axial load at the limit point of each equilibrium path (Nagarajaiah and Ferrell 1999). This procedure was repeated for increasing values of initial shear displacement; the corresponding critical load—horizontal displacement values were obtained. Complete details of the finite element model and analysis results can be found in Liu et al. (2002).

Evaluation of Analysis Results

The variation of normalized critical load with normalized horizontal displacement computed using the ADINA finite element program is presented in Figs. 10 and 11, for the 100, 200, 300 and 400, 500, 600 bearing series, respectively. The results from the nonlinear analytical model developed by Nagarajaiah and Ferrell (1999) in a companion paper are also shown for the same set of bearings. The comparisons with ADINA results for 100 and 400 series bearings are not shown, as reliable results could not be obtained due to convergence problems experienced in the finite element solution for these bearings. The critical load at a given shear displacement is normalized with respect to the critical load at zero-shear displacement. Similarly, the horizontal displacement is normalized with respect to the width of the bearing. This is

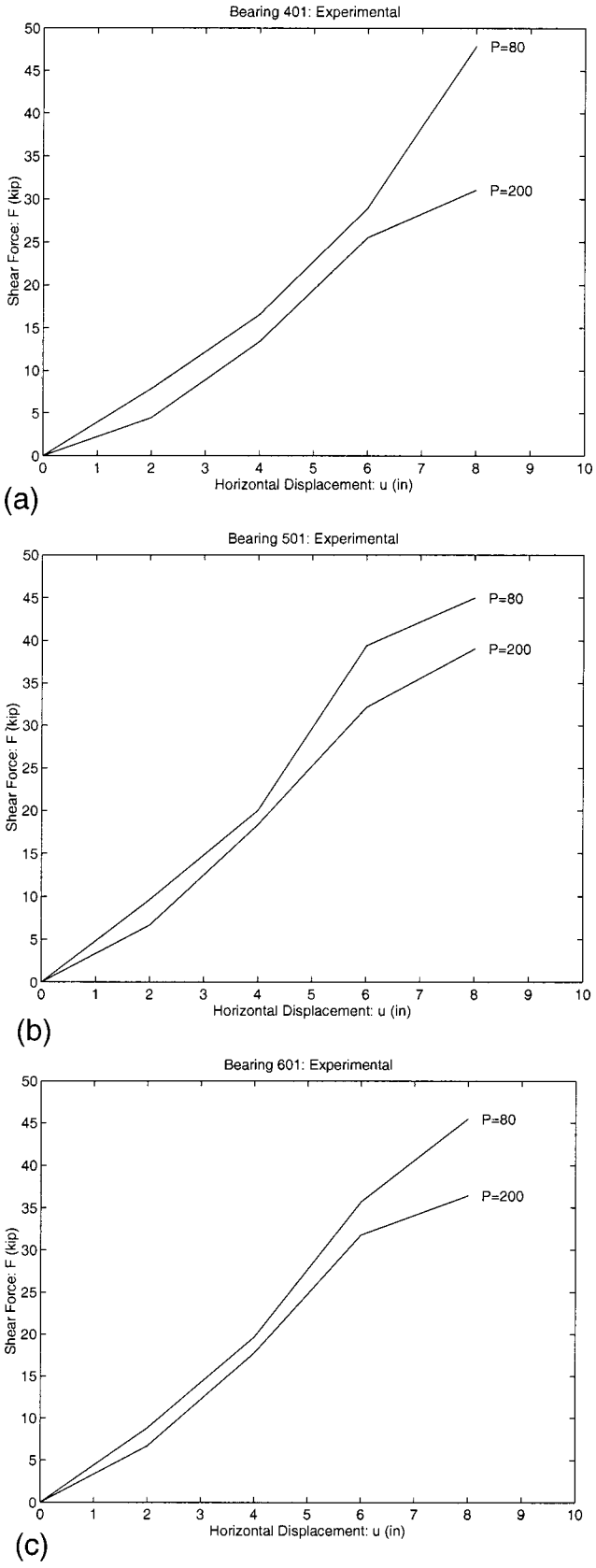

Fig. 8. Stability test: Shear force–displacement curves as function of axial load (a) bearing 401; (b) bearing 501, and (c) bearing 601

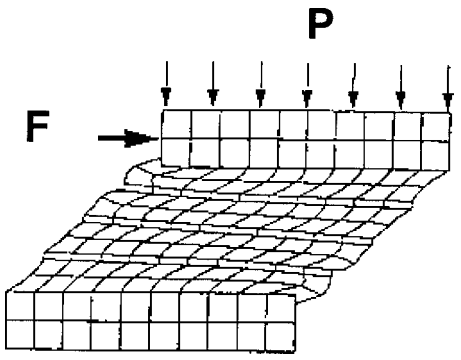

Fig. 9. Finite element model subjected to constant shear force, F, and monotonically increasing axial force, P

necessary since in the finite element analysis, strip bearings of unit breadth were analyzed under plane strain condition. Hence, the results cannot be compared directly since the actual breadth of the bearings is either 5 in. (127 mm) or 10 in. (254 mm). The comparison in Figs. 10 and 11 indicate good agreement for both 5 in. (127 mm) and 10 in. (254 mm) bearings with different shape factors. The reduction in critical load with increasing horizontal displacement is captured in both the analytical model results and the ADINA results. The comparisons indicate that the effect of large horizontal displacements on the critical load can be reliably predicted. It is worth noting that a two degree of freedom nonlinear analytical model (Nagarajaiah and Ferrell 1999) can capture the complex nonlinear behavior adequately as compared to the finite element model.

It is evident from the results in Figs. 10 and 11 that substantial critical load capacity exists at a horizontal displacement equal to the width of the bearing and is not zero, as predicted by the correction factors used in design to account for large shear displacements. These factors are not conservative at smaller displacements and overly conservative at larger displacements.

It is also important to note that 200 series bearings with shape factor, $S=2.5$, and rubber layer thickness, $t=0.5$ in. (12.7 mm) exhibits a similar reduction in critical load with horizontal displacement, as compared to 500 series bearings with $S=5$, and $t=0.5$ in. (12.7 mm). A similar observation can be made when the results of 100, 300 series bearings and 400, 600 series bearings are compared. Hence, the rubber layer thickness seems to have stronger influence than the shape factor on the decrease in the critical load with horizontal displacement. This same observation may be made from the data in Table 2. In this table the ratio of P_{cr} (at $u=B$) to P_{cr} (at $u=0$) is given for each of the bearings. These data are obtained from Figs. 10 and 11, and based on analytical results for series 400 from Nagarajaiah and Ferrell (1999). Again it may be seen that the critical load ratio at $u=B$, decreases with decreasing layer thickness. It might also be said that this ratio decreases with increasing shape factor but the trend is inconsistent. There is a stronger relationship between critical load ratio and layer thickness than with shape factor.

Conclusions

Experiments performed on a series of elastomeric bearings have been presented. Tests were performed with specific objectives of finding the effect of horizontal displacement or shear strain on the critical load and to evaluate the existing design approaches. Analytical predictions were made.

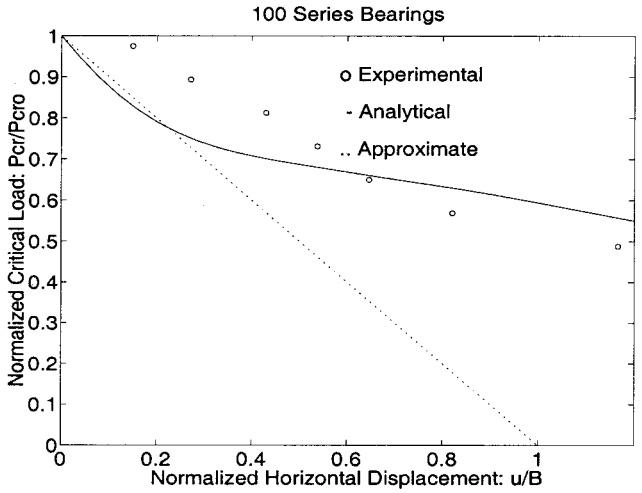

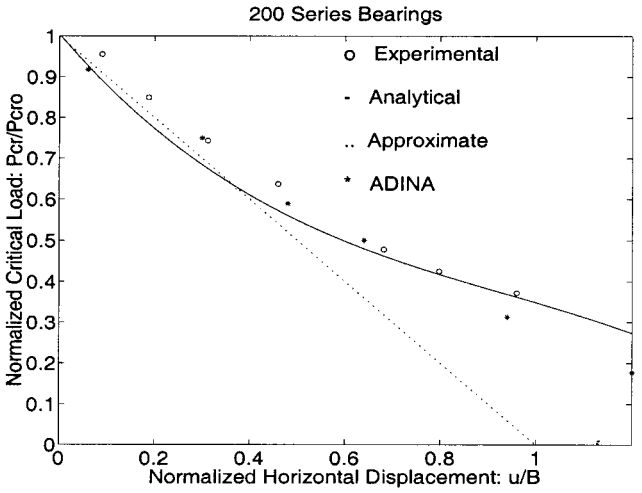

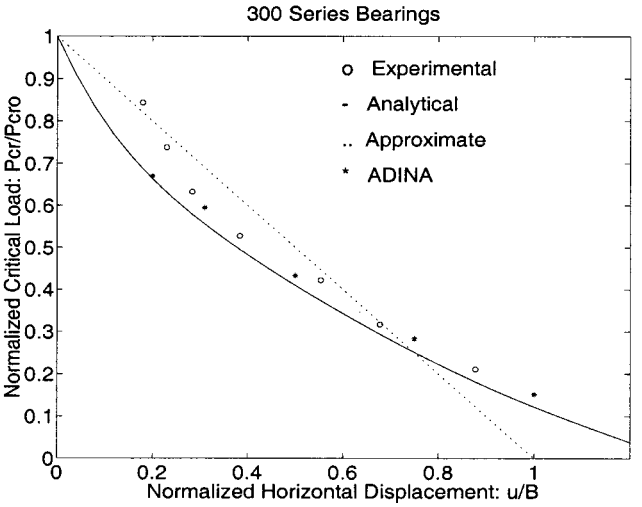

Fig. 10. Critical load as function of horizontal displacement

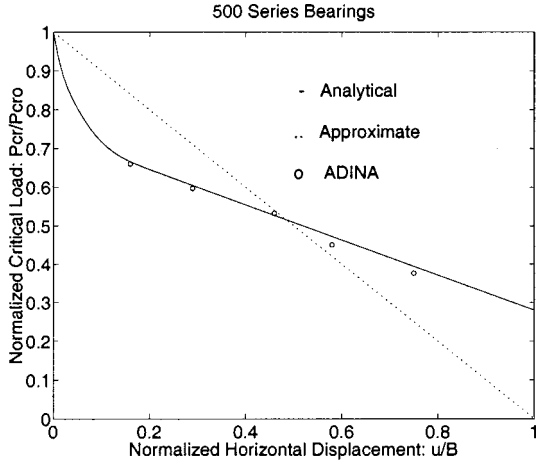

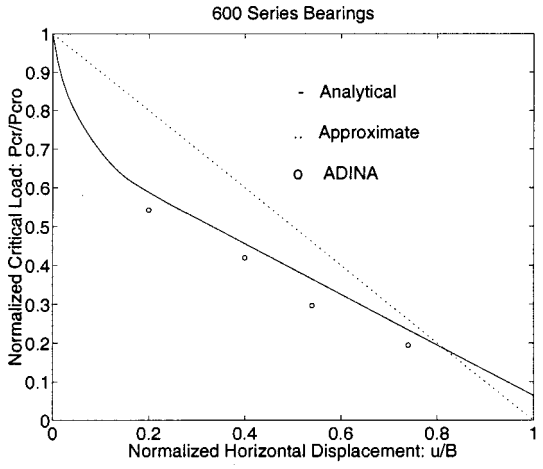

Fig. 11. Critical load as function of horizontal displacement

The conclusions based on the test results and the analysis results are as follows:

1. The critical load decreases with increasing horizontal displacement or shear strain;
2. The horizontal stiffness decreases with increasing axial load and horizontal displacement;
3. Moment is a nonlinear function of displacement and the moment resisting capability increases with increasing axial load;
4. Height reduction of the bearing increases with increasing horizontal displacement and axial load;
5. Substantial critical load capacity exists at a horizontal displacement equal to the width of the bearing and is not equal to zero, as predicted by the correction factors used in design;
6. The correction factors are not conservative at smaller displacements and overly conservative at larger displacements; and
7. The rubber layer thickness seems to have greater influence than the shape factor on the decrease in the critical load with horizontal displacement.

Table 2. Critical Load Ratios at $u = B$

Bearing series	Shape factor S	Rubber layer thickness t	Critical load ratio P_{cr}/P_{cr0}
100	1.67	0.75	0.59
400	3.33	0.75	0.55
200	2.50	0.50	0.35
500	5.00	0.50	0.28
300	5.00	0.25	0.12
600	10.00	0.25	0.07

The aforementioned conclusions are based on a limited set of experimental results of bearings with relatively low shape factors. Further experimental studies are necessary to evaluate bearings with larger shape factors.

Acknowledgments

Funding for this project provided by the Multidisciplinary Center for Earthquake Engineering Research and the Federal Highway Administration is gratefully acknowledged. The bearing tests were conducted by the first writer in collaboration with Professor James Kelly at the Earthquake Engineering Research Center. The assistance of Dr. Peter Clark in recovering the raw test data is gratefully acknowledged. The writers also acknowledge the assistance of Dr. Helen Liu who performed the ADINA analyses. The bearings were manufactured and supplied by Dynamic Isolation Systems, Lafayette, CA.

References

ADINA (1999). A finite Element Program for Automatic Dynamic Incremental Nonlinear analysis, ADINA R&D Inc., Watertown, Mass.

Buckle, I. G., and Kelly, J. M. (1986). ''Properties of slender elastomeric isolation bearings during shake table studies of a large-scale model bridge deck.'' Joint Sealing and Bearing Systems for Concrete Structures (American Concrete Institute), 1, 247–269.

Buckle, I. G., and Liu, H. (1993). ''Stability of elastomeric seismic isolation systems,'' *Proc., Seminar on Seismic Isolation, Passive Energy Dissipation and Control*, ATC-17-1, Applied Technology Council, Calif., 293–305.

Buckle, I. G., and Liu, H. (1994). ''Experimental determination of critical loads of elastomeric isolators at high shear strain.'' *NCEER Bull.*, 8(3), 1–5.

Haringx, J. A. (1948). ''On highly compressive helical springs and rubber rods and their applications for vibration-free mountings. I.'' *Philips Res. Rep.*, 3, 401–449.

Haringx, J. A. (1949a). ''On highly compressive helical springs and rubber rods and their applications for vibration-free mountings. II.'' *Philips Res. Rep.*, 4, 49–80.

Haringx, J. A. (1949b). ''On highly compressive helical springs and rubber rods and their applications for vibration-free mountings. III.'' *Philips Res. Rep.*, 3, 206–220.

Koh, C. G., and Kelly, J. M. (1986). ''Effects of axial load on elastomeric bearings,'' *Rep. UCB/EERC-86/12*, Earthquake Engineering Research Center, Univ. of California, Berkeley, Calif.

Nagarajaiah, S., and Ferrell, K. (1999). ''Stability of elastomeric seismic isolation bearings.'' *J. Struct. Eng.*, 125(9), 946–954. structures: Part II.'' *Rep. NCEER-91-0005*, National Center for Earthquake Engineering Research, SUNY, Buffalo, NY.